Pecora Escarpment 02007

Anorthositic regolith breccia

22.4 g

Figure 1: PCA 02007 as found in the ice near Pecora Escarpment (left), and the underside held upside down with stainless steel tongs by J. Schutt (right).

Introduction

Pecora Escarpment (PCA) 02007 was found in Antarctica by the 2002-2003 ANSMET team (Fig. 1) on January 5, 2003 in the N40 icefield region (Fig. 2). It's distinctive greenish and frothy (in places) fusion crust hinted at a lunar origin even in the field. It is also very thin with the top side showing brownish fusion crust and the under side showing more frothy greenish crust. Although initially described as a basalt regolith breccia based on examination of thin section ,4, studies of additional sections have led to the realization that this is a feldspathic regolith breccia.

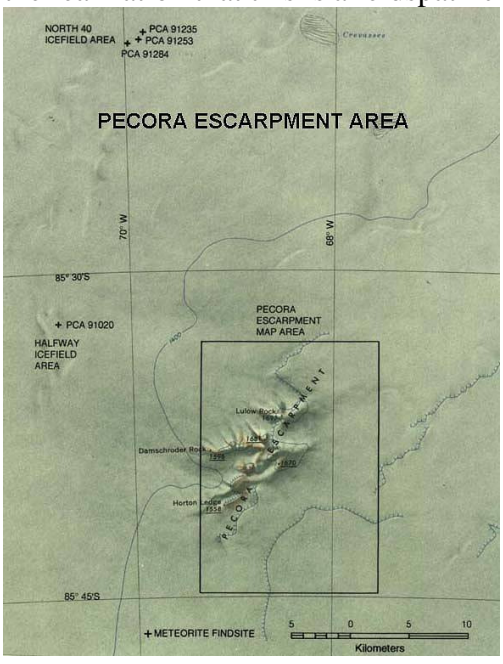

Figure 2: The Pecora Escarpment region of Antarctica, with the N40 icefield (where PCA 02007 was found) shown at the north edge of the map.

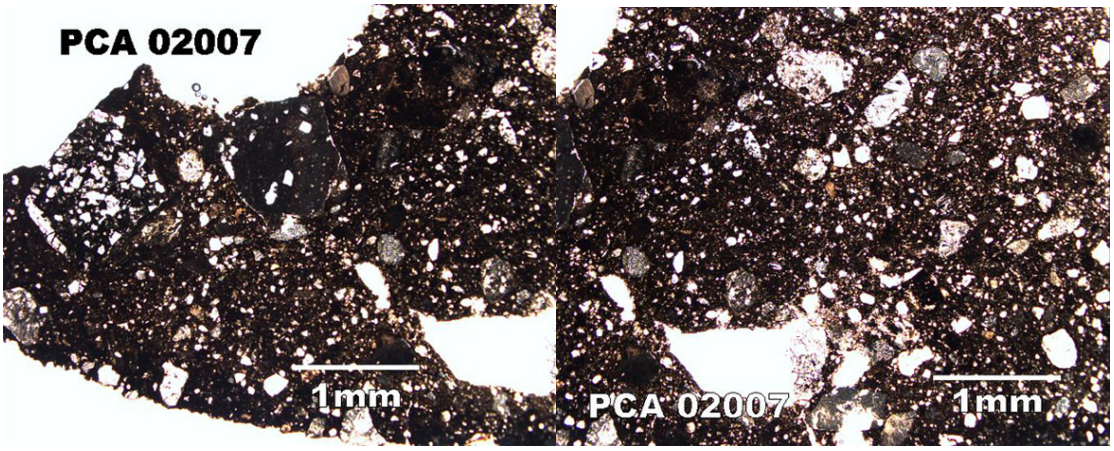

Figure 3: Low magnification plane polarized light images of section PCA 02007 ,4. Most of the light colored clasts are plagioclase-rich.

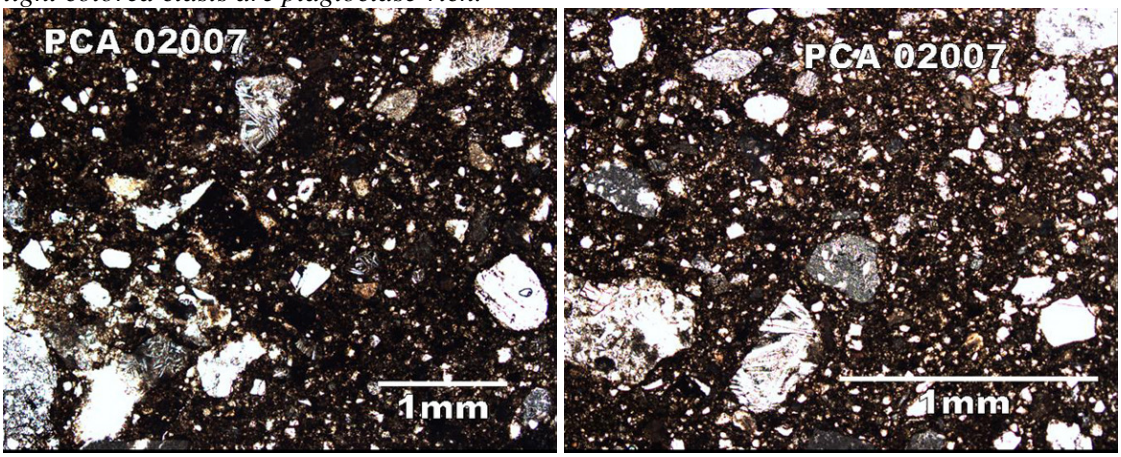

Figure 4: Higher magnification plane polarized light images of section PCA 02007 ,4. Again, most of the light colored clasts are plagioclase-rich with glasses and mineral fragments also present.

Petrography and Mineralogy

PCA 02007 is a breccia comprised of mineral, glass and lithic clasts (Figs. 3 and 4), some of which are up to 3 mm in size (Zeigler et al., 2004; Taylor et al., 2004; Korotev et al., 2006). Lithic clasts are mainly plagioclase-rich, and occur in several different textures: plagioclase/glass intergrowths, intergranular, quenched texture, and regolith breccia clasts. Backscattered electron images of several such clasts are shown in Fig. 5, 6 and 7 (from Korotev et al., 2006). There are also rare very low Ti basalt clasts found in PCA 02007 (Taylor et al., 2004), but these are minor compared to the feldspathic clasts. Mineral fragments are mainly plagioclase, but also include pyroxene, olivine, silica, ilmenite, spinel, troilite, and FeNi metal. Pyroxenes are largely magnesian and calcic, typical of high magnesium suite highlands rocks (Fig. 8). There are also more ferroan pyroxenes in a few basaltic clasts (Fig. 8), similar to other Apollo mare basalt pyroxenes compositions. Glassy clasts have a wide range of bulk compositions but most reflect a large feldspathic component, with high Al_2O_3, and low to intermediate FeO (Fig. 9).

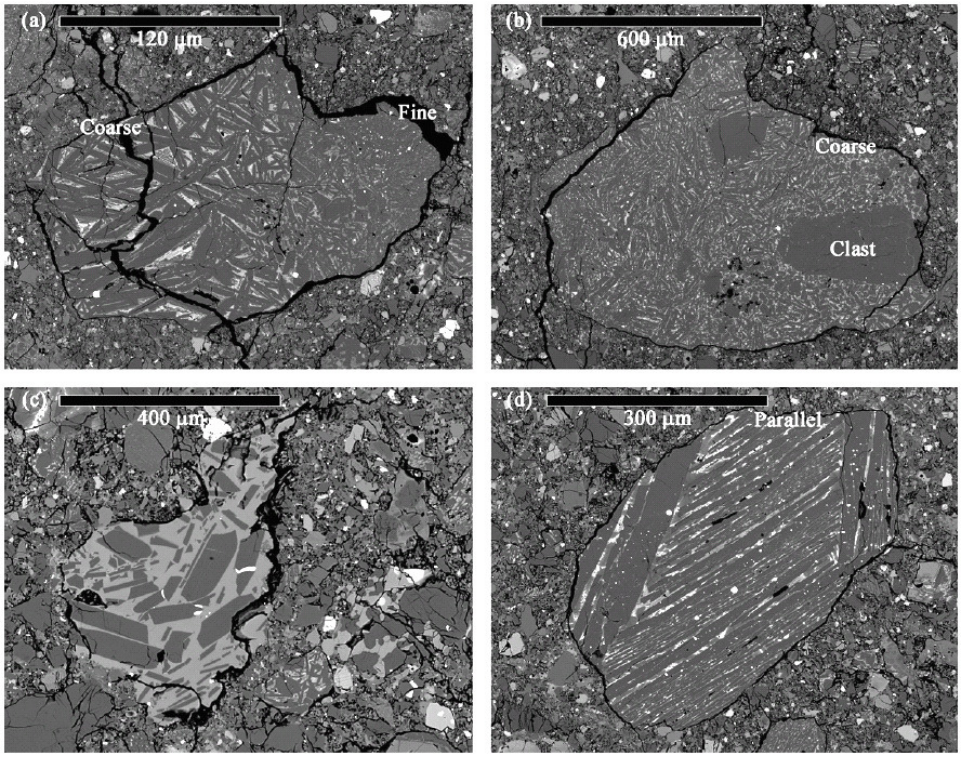

Figure 5: Back scattered electron (BSE) images of plagioclase-rich clasts from PCA 02007 illustrating quenched texture indicating a probable impact melt origin (from Korotev et al., 2006). Plagioclase is the dark phase is all images.

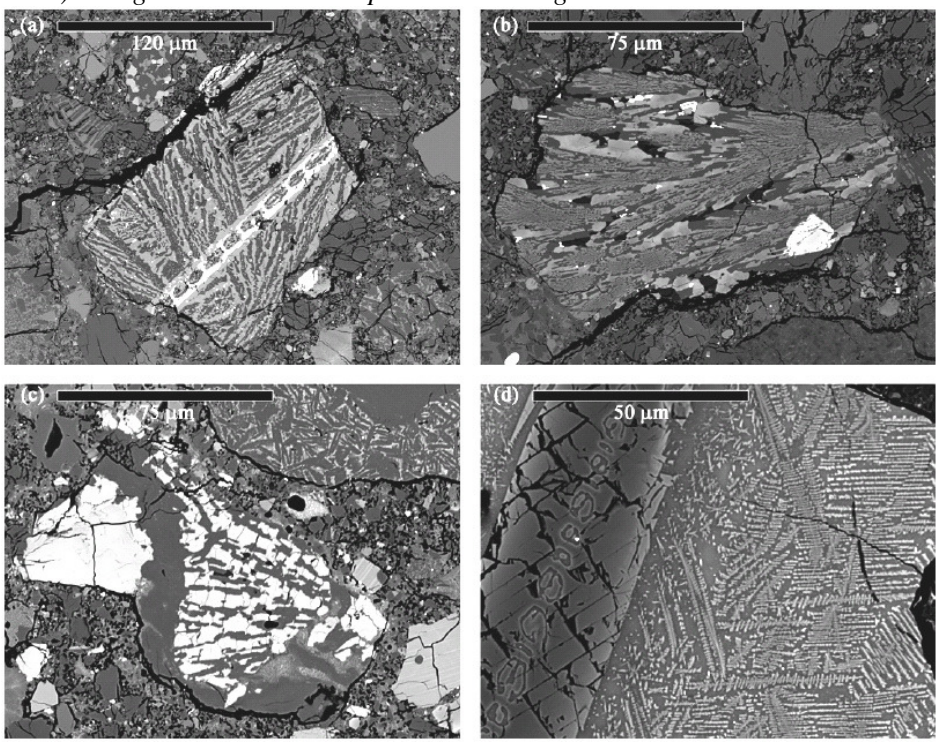

Figure 6: Back scattered electron (BSE) images of mafic lithic clasts from PCA 02007 illustrating typical dendritic and skeletal textures formed by quenching (from Korotev et al., 2006). Phases in images: (a) olivine, plagioclase, pyroxene, and melt (b) plagioclase, pyroxene, silica, chromite, and melt (brightest), (c) pyroxene and plagioclase, and melt (d) olivine and melt.

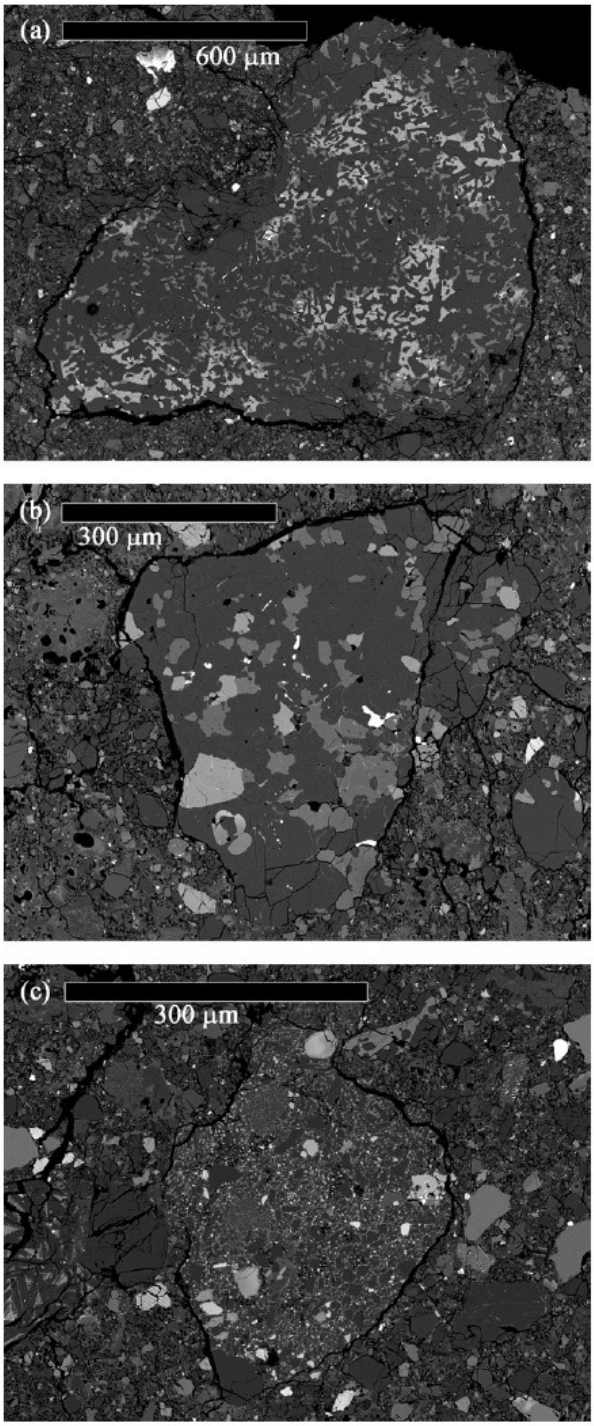

Figure 7: Three BSE images of plagioclase- and pyroxene-bearing intergranular textured (a and b) clasts and a regolith breccia lithic clast (c) (from Korotev et al., 2006).

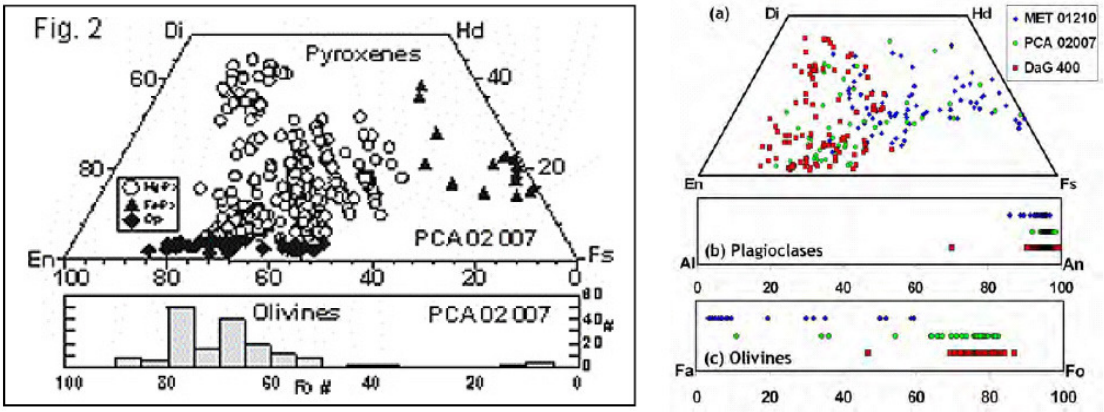

Figure 8: Pyroxene and olivine compositions for clasts and fragments analyzed by Taylor et al. (2004) in section ,27 (left), as well as plagioclase, olivine and pyroxene from section ,34.

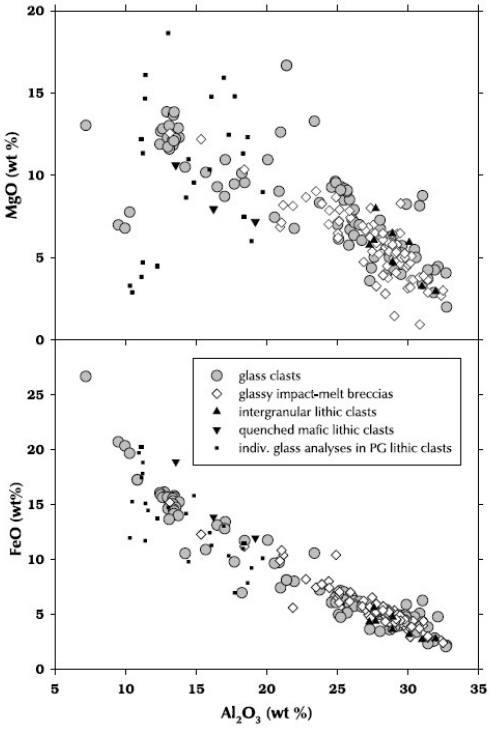

Figure 9: Glass and lithic clast compositions from section 23 of PCA 02007, illustrating the dominantly aluminous (feldspathic) nature of the glasses (from Korotev et al., 2006).

Chemistry

PCA 02007 has a bulk composition that is more mafic than most feldspathic lunar meteorites, but it is clearly feldspathic and contains only little petrographic and compositional evidence for a mare component (Table 1 and Figs. 10-13). For example, La/Yb is low and Cr and FeO contents are among the highest for feldspathic lunar meteorites, but Al_2O_3 is still high > 26 wt% (Figs. 10 and 11) and CaO/ Al_2O_3 are low (Fig. 12). High siderophile element concentrations suggest a derivation from mature regolith, similar to that proposed for QUE 93069. In addition, this sample and other lunar meteorite regolith breccias have higher Sm and other incompatible elements (Fig. 13; Korotev et al., 2006). Overall similarities between Yamato 791197 and PCA 02007 led

Zeigler et al. (2004) to propose a launch pairing of these two meteorites. However, this is inconsistent with new compositional data (Cr/Sc; Fig. 13), as well as cosmogenic exposure age dating constraints (see below).

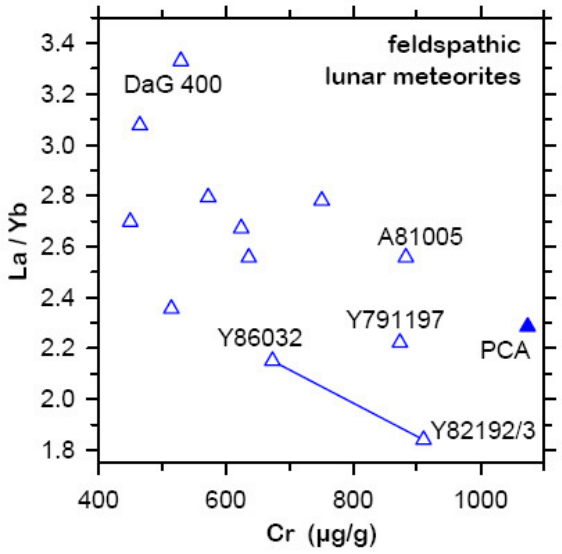

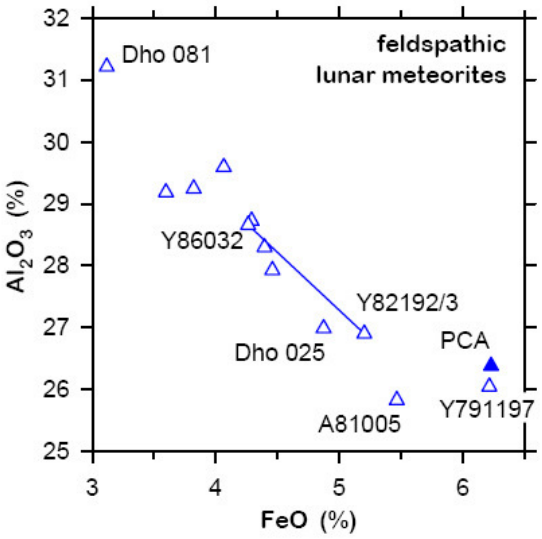

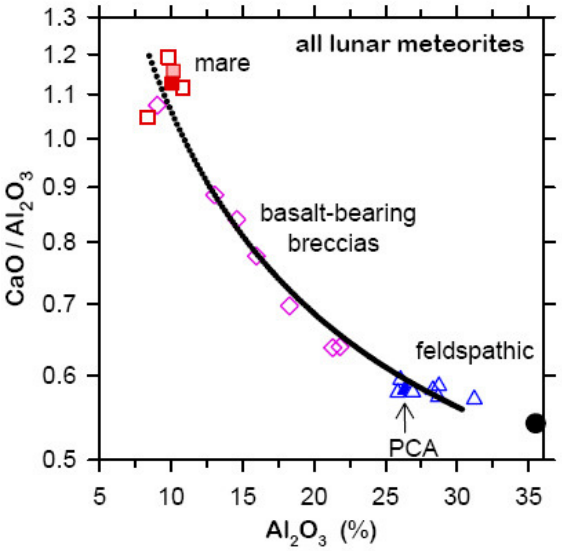

Figure 10: La/Yb vs. Cr for feldspathic lunar meteorites (from Korotev et al., 2004). Figure 11: Al_2O_3 vs. FeO for feldspathic lunar meteorites illustrating the higher FeO contents of PCA 02007 compared to other feldspathic lunar meteorites. Figure 12: CaO/ Al_2O_3 vs. Al_2O_3 for mare, mingled, and feldspathic meteorites showing that PCA 02007 falls within the range previously defined for feldspathic lunar meteorites (from Korotev et al., 2004).

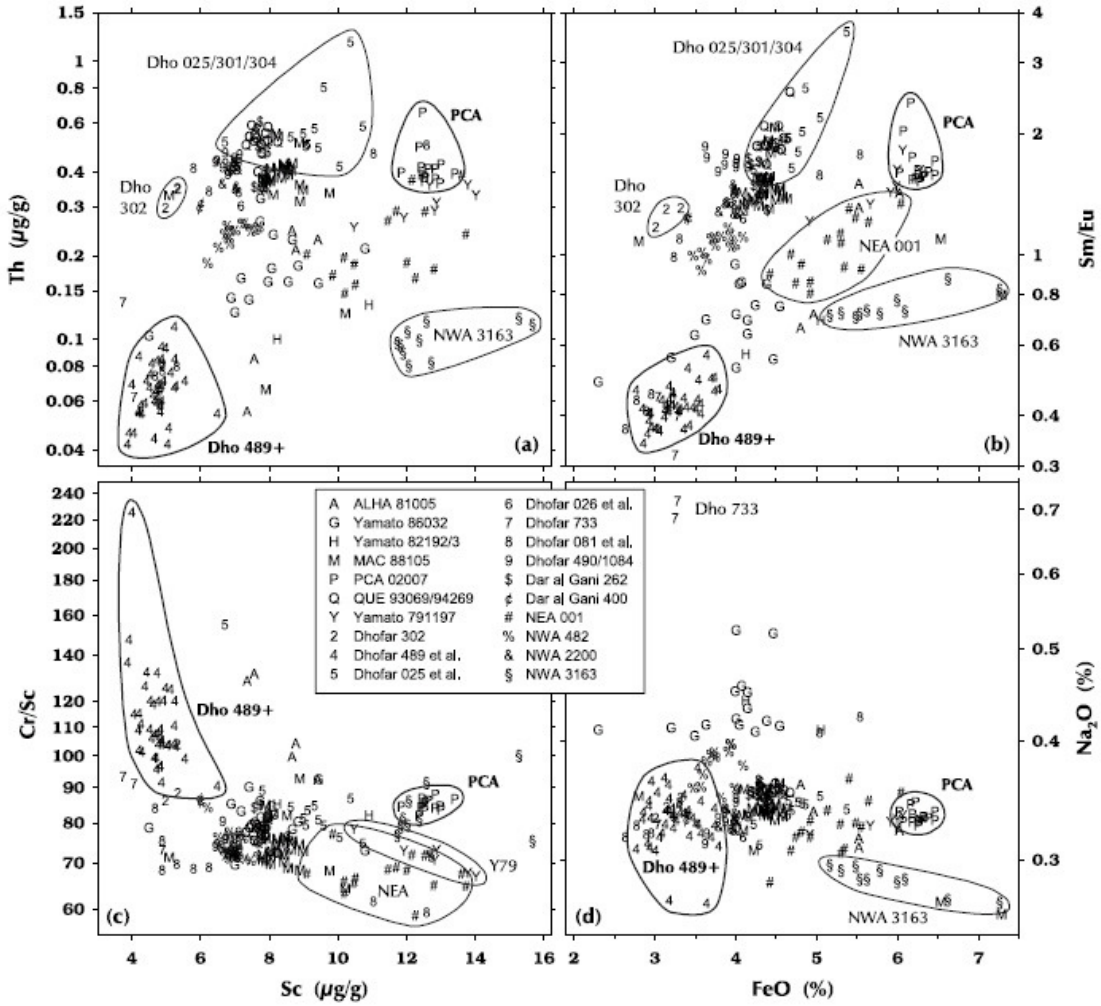

Figure 13: Chemical composition of many sub-samples from PCA 02007 illustrating their slightly higher, Sc and FeO concentrations relative to other feldspathic lunar meteorites (from Korotev et al., 2006).

Table 1. Chemical composition of PCA 02007

reference	1	2	3	3	3	3	3	4	5
weight	535	312	16	21	34	12	avg.	493.6	50
method	b	a,b	e	e	e	e	e	d,e	b
SiO_2 %	38.6	43.41	44.2	44.5	44.7	44.9	44.6	44.8	38.6
TiO_2	0.28	0.28	0.28	0.29	0.28	0.29	0.28	0.286	0.28
Al_2O_3	29.06	25.71	26.2	26.9	26.4	25.7	26.4	26.5	29.1
FeO	6.8	6.3	6.42	6.24	6.25	6.15	6.26	6.26	6.8
MnO	0.09	0.09	0.07	0.09	0.09	0.11	0.09	0.09	0.09
MgO	7.4	6.8	6.8	6.2	6.7	7.3	6.7	6.7	7.4
CaO	17.26	15.19	15.3	15.6	15.3	15	15.3	15.4	17.3
Na_2O	0.38	0.36	0.34	0.33	0.33	0.28	0.33	0.333	0.38
K_2O	0.05	0.03	0.02	0.03	0.02	0.02	0.02	0.021	0.05
P_2O_5	0.08	0.03	0.03	0.03	0.02	0.03	0.03	0.027	0.08
S %									
sum								100.14	
Sc ppm	11.8	13						12.65	7.95
V	50.6	32							48.2
Cr		1168	1163	1026	1026	1095	1095	1075	656
Co	29.8	27						29.2	23
Ni	353.67	324						354	292
Cu		11							4.77
Zn		17							10.9
Ga	3.86	3.14							2.33
Ge									
As									
Se									
Rb	0.82	0.588							0.56
Sr	151.5	144						147	140
Y	9.77	11							8.23
Zr	40.2	58						36	32.2
Nb	2.5	2.64							2.55
Mo		0.413							
Ru									
Rh									
Pd ppb									
Ag ppb									
Cd ppb									
In ppb									
Sn ppb									
Sb ppb									
Te ppb									
Cs ppm	0.09	0.047							0.06
Ba	34.8	70						34	33.4
La	2.67	2.52						2.55	2.49
Ce	7.69	6.21						6.85	7.11

Pr	1.06	0.888		0.97
Nd	5.28	4.19	4.2	4.78
Sm	1.89	1.22	1.269	1.56
Eu	0.9	0.88	0.763	0.77
Gd	2.13	1.44		1.79
Tb	0.4	0.287	0.282	0.36
Dy	2.1	1.81		1.86
Ho	0.45	0.393		0.4
Er	1.33	1.16		1.04
Tm	0.19	0.164		0.15
Yb	1.29	1.11	1.117	1.07
Lu	0.2	0.164	0.157	0.15
Hf	1.33	0.83	0.94	1.07
Ta	0.24	0.176	0.135	0.21
W ppb	200			
Re ppb				
Os ppb				
Ir ppb			16.8	
Pt ppb				
Au ppb			6.7	
Th ppm		0.37	0.41	0.47
U ppm		0.107	0.11	0.14

technique (a) ICP-AES, (b) ICP-MS, (c) IDMS, (d) FB-EMPA, (e) INAA, (f) RNAA

Table 1b. Light and/or volatile elements for PCA 02007

Li ppm		4	4.23
Be	0.5	0.257	0.44
C			
S			
F ppm			
Cl			
Br			
I			
Pb ppm	1.16	0.835	0.71
Hg ppb			
Tl		0.051	
Bi			

1) Taylor et al. (2004); 2) Joy et al. (2006); 3) Zeigler et al. (2004); 4) Korotev et al. (2006); 5) Day et al. (2006)

Radiometric age dating

None yet reported.

Cosmogenic exposure ages

Cosmogenic exposure age dating has yielded a ^{10}Be (4π) ejection age of 0.95 Ma (Nishiizumi et al., 2006). A terrestrial age of 30 Ka was also determined by this study. The ejection age of < 0.1 Ma determined for Yamato 791197 is younger than that for PCA 02007, inconsistent with a launch pairing suggested by Zeigler et al. (2004).

Processing

PCA 02007 has been processed in several stages with the initial processing including thin sections and oxygen isotopes, and later processing including allocation of many additional chips and thin sections (Table 2 and Figures 14 to 17).

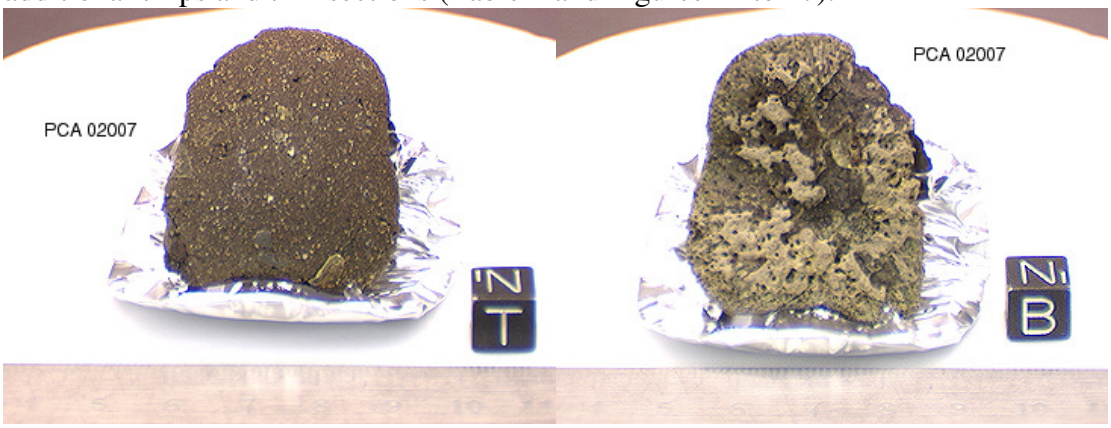

Figure 14 and 15: Top and bottom views of PCA 02007 in the Meteorite Processing Lab, JSC.

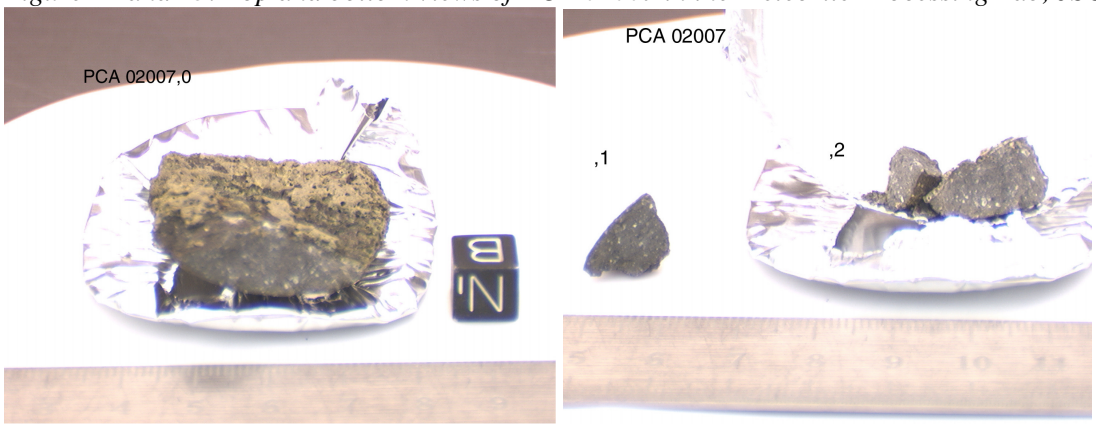

Figure 16 and 17: North and post initial processing (splits 1 and 2) views of PCA 02007 in the Meteorite Processing Lab, JSC.

Table 2. Allocation history of PCA 02007 (July, 2006)

split	TS	parent	mass	PI/location	comment
0		0	7.799	JSC	Documented chip
1		0		Entirely subdivided	Potted butt
	4		0.01	McCoy/SI	Thin section
	5		0.01	Warren	Thin section
	23		0.01	Korotev	Thin section
2		0	0.679	JSC	Chips and fines
6		2	0.148	Clayton	Interior chip
8		2		entirely subdivided	Potted butt
	24		0.01	Taylor (LA)	Thin section
	25		0.01	Arai	Thin section
	26		0.01	Korotev	Thin section
	27		0.01	Taylor (LA)	Thin section
	34		0.01	Russell	Thin section

10		0	0.596	Nishiizumi	Locatable exterior chip
11		0	0.112	Korotev	Locatable interior chip
12		0	0.204	Arai	Locatable interior chip
13		0	0.535	Taylor (LA)	2 locatable chips
14		0	0.169	Korotev	Locatable chip
15		0	0.521	Nishiizumi	Locatable interior chip
16		0	0.233	Korotev	Locatable interior chip
17		0	2.507	JSC	Chips and fines
28		17	0.093	Korotev	Exterior chip
31		17	0.118	Busemann	Interior chip
32		17	0.303	Herzog	Interior chip
36		0	0.933	JSC	Potted butt
	42		0.01	Taylor (GJ)	Thin section
	43		0.01	Terada	Thin section
37		0	0.312	Russell	2 interior chips
38		0	3.559	JSC	Chips and fines
40		38	0.511	Warren	Interior chips
44		17	0.070	Podosek	Interior chip